Acta Crystallographica Section D
Biological Crystallography
ISSN 0907-4449

Mycobacterium tuberculosis pantothenate kinase: possible changes in location of ligands during enzyme action

Bhaskar Chetnani,[a]‡ Satyabrata Das,[a]‡ Parimal Kumar,[a] A. Surolia[a,b] and M. Vijayan[a]*

[a]Molecular Biophysics Unit, Indian Institute of Science, Bangalore 560012, India, and [b]National Institute of Immunology, Aruna Asaf Ali Marg, New Delhi 110067, India

‡ These authors contributed equally to this work.

Correspondence e-mail: mv@mbu.iisc.ernet.in

Received 24 September 2008
Accepted 16 January 2009

PDB References: *Mt*PanK, initiation complex, 2zse, r2zsesf; intermediate complex, 2zsf, r2zsfsf; end complex, 2zsa, r2zsasf; citrate complex, 2zs7, r2zs7sf; complex with ADP and pantothenate, 2zs9, r2zs9sf; complex with CoA, 2zsd, r2zsdsf; complex with ADP (cocrystallized), 2zs8, r2zs8sf; complex with ADP (soaked), 2zsb, r2zsbsf.

The crystal structures of complexes of *Mycobacterium tuberculosis* pantothenate kinase with the following ligands have been determined: (i) citrate; (ii) the nonhydrolysable ATP analogue AMPPCP and pantothenate (the initiation complex); (iii) ADP and phosphopantothenate resulting from phosphorylation of pantothenate by ATP in the crystal (the end complex); (iv) ATP and ADP, each with half occupancy, resulting from a quick soak of crystals in ATP (the intermediate complex); (v) CoA; (vi) ADP prepared by soaking and cocrystallization, which turned out to have identical structures, and (vii) ADP and pantothenate. Solution studies on CoA binding and catalytic activity have also been carried out. Unlike in the case of the homologous *Escherichia coli* enzyme, AMPPCP and ADP occupy different, though overlapping, locations in the respective complexes; the same is true of pantothenate in the initiation complex and phosphopantothenate in the end complex. The binding site of *Mt*PanK is substantially preformed, while that of *Ec*PanK exhibits considerable plasticity. The difference in the behaviour of the *E. coli* and *M. tuberculosis* enzymes could be explained in terms of changes in local structure resulting from substitutions. It is unusual for two homologous enzymes to exhibit such striking differences in action. Therefore, the results have to be treated with caution. However, the changes in the locations of ligands exhibited by *M. tuberculosis* pantothenate kinase are remarkable and novel.

1. Introduction

Coenzyme A (CoA) is an important and essential cofactor that is involved in many biological processes. The first step in its biosynthesis is the ATP-mediated phosphorylation of pantothenate (vitamin B_5) by pantothenate kinase (PanK; Leonardi *et al.*, 2005). Apart from the classical PanK (type I) from *Escherichia coli*, two other types of pantothenate kinase (type II and type III) have been identified in bacteria (Choudhry *et al.*, 2003; Brand & Strauss, 2005). These enzymes exhibit wide variations in their distribution, mechanisms of regulation and affinity for substrates. While the type I enzyme is found exclusively in eubacterial species and is feedback-regulated by CoA, all type III PanKs characterized to date are not inhibited by CoA (Yang *et al.*, 2006). The type II enzymes, on the other hand, are also regulated by CoA, although there are a few exceptions. Many pathogenic bacteria, including *Helicobacter pylori*, *Bordetella pertussis*, *Pseudomonas aeruginosa* and *Francisella tularensis*, have only type III PanK, whereas *Bacillus subtilis* and *Mycobacterium tuberculosis* have both type I and type III enzymes. In *S. aureus*, type II PanK is the only pantothenate kinase, whereas *Bacillus anthracis* and

B. cereus contain both type II and III PanKs. PanK from *S. aureus* is most similar in sequence to the mammalian PanK catalytic core (23% sequence identity), but unlike *S. aureus* PanK mammalian PanK it is feedback-regulated by CoA and its thioesters (Hong *et al.*, 2007). In mammals (such as humans and mouse) four PANK genes are found which code for different isoforms of pantothenate kinase that exhibit a wide variation in length, composition and in tissue-specific expression (Zhou *et al.*, 2001; Zhang *et al.*, 2006). They also differ substantially in sequence from bacterial PanK, which is a key regulatory enzyme in maintaining the intracellular concentration of CoA in bacteria (Cheek *et al.*, 2005). Therefore, PanK is considered to be a good target for the development of antibacterials.

Type I PanK from *E. coli* (*Ec*PanK) has been extensively structurally characterized through X-ray analysis of its complexes with CoA, with 5′-adenylimidodiphosphate (AMPPNP), which is a nonhydrolysable analogue of ATP, and with ADP and pantothenate (Yun *et al.*, 2000; Ivey *et al.*, 2004). The homodimeric enzyme (Song & Jackowski, 1994) has a subunit consisting of 316 amino-acid residues. Each subunit has a mononucleotide-binding fold with a seven-stranded β-sheet flanked by helices. It is a P-loop kinase. The CoA- and ATP-binding sites in each subunit overlap. Local conformational differences exist between the *Ec*PanK complexes of CoA and ATP. Pantothenate binding also involves a local conformational change. These structures and associated data have provided insight into the mechanism of action of *Ec*PanK.

Recently, we have reported the structure of the CoA complex of the type I enzyme from *Mycobacterium tuberculosis*, the causative agent of TB, as part of a programme in this laboratory on structural studies of mycobacterial proteins (Das *et al.*, 2006; Vijayan, 2005; Krishna *et al.*, 2007; Selvaraj *et al.*, 2007; Roy *et al.*, 2008). The structure of *M. tuberculosis* PanK (*Mt*PanK) is very similar to that of *Ec*PanK although differences exist, particularly at the inter-subunit interface in the dimer. However, the CoA-binding region in the two enzymes is almost entirely conserved. Comparisons involving sequences suggest that this is true for the enzyme from different bacterial sources. Here, we report the crystal structures of the native enzyme with citrate molecules from the buffer in the active site and of several ternary and binary complexes of *Mt*PanK. One of the ternary complexes involves AMPPCP, a nonhydrolysable analogue of ATP similar to AMPPNP, and pantothenate. A second ternary complex was obtained by soaking crystals of the enzyme in a solution containing ATP and pantothenate and involves ADP and phosphopantothenate. The two complexes therefore represent the beginning and the end of the enzymatic reaction. The third complex was obtained by soaking the crystals for a very short time in ATP. ATP is partially hydrolysed and the active site appears to contain ATP and ADP in equal proportions, providing a possible picture of an intermediate state during the reaction. A fourth complex, again obtained by soaking, involves ADP and pantothenate. A binary complex with ADP was obtained by soaking as well as by cocrystallization. Yet another binary complex, prepared by soaking, was with CoA. These structures suggest substantial changes in the locations of ligands during enzyme action, unlike in the case of *Ec*PanK. Also, unlike that of *Ec*PanK, the structure of *Mt*PanK remains relatively unchanged during complexation. Thus, although the two enzymes are homologous, they apparently act in somewhat different ways.

2. Material and methods

2.1. Cloning, expression and purification

The cloning, expression and purification of *Mt*PanK have been reported previously (Das *et al.*, 2005). Recombinant *Ec*PanK was cloned, expressed and purified in a similar way. Briefly, the PCR-amplified genomic DNA for *Ec*PanK was cloned into the pET-28a expression vector with His_6 at the N-terminus. The cloned gene was then transformed into *E. coli* BL21 (DE3) cells. The cells were grown in LB medium and induced using IPTG (0.2 m*M*). A single-step purification of the recombinant protein was performed using an Ni–NTA metal-affinity column. Purified *Mt*PanK and *Ec*PanK were dialyzed into 0.1 *M* Tris–HCl buffer consisting of 0.2 *M* NaCl, 10% glycerol pH 8.0 for 24 h.

2.2. Removal of bound CoA from *Mt*PanK

The method used in the case of phosphopantetheine adenyltransferase (Geerlof *et al.*, 1999) with some optimization was employed for removing the protein-bound CoA from *Mt*PanK. The purified recombinant protein was subjected to extensive dialysis successively against 0.1 *M* citrate buffer, 0.2 *M* NaCl, 10% glycerol pH 5.6 (24 h), 0.1 *M* citrate buffer, 0.3 *M* NaCl and 10% glycerol pH 5.0 (3 d with a buffer change every 24 h) and 0.1 *M* citrate buffer, 0.2 *M* NaCl and 10% glycerol pH 5.6 (24 h). The precipitated protein at the end of dialysis was removed by centrifugation and the supernatant was applied onto an FPLC Sephadex G25 column (Amersham Biosciences). The protein fractions thus obtained were then concentrated using Amicon membranes (10 kDa cutoff).

2.3. Isothermal titration calorimetry (ITC) of *Mt*PanK and *Ec*PanK with CoA

All the experiments were performed in a VP-ITC MicroCalorimeter (MicroCal Inc., Northampton, Massachusetts, USA) at 293 K. For each experiment, purified *Mt*PanK or *Ec*PanK was dialyzed against 0.1 *M* Tris–HCl buffer, 0.2 *M* NaCl, 10% glycerol pH 8.0 for 24 h with one change. For CoA-free *Mt*PanK, 0.1 *M* citrate buffer pH 5.6 was used instead. The ligand (CoA) solution was prepared in the respective dialysis buffer. The sample cell (volume 1.4 ml) was filled with 90, 68 and 14 μM of purified dimeric *Mt*PanK, *Ec*PanK and CoA-free *Mt*PanK, respectively. The corresponding concentrations of CoA in the ITC syringe (volume 298 µl) for purified *Mt*PanK, *Ec*PanK and CoA-free *Mt*PanK were 2.8, 1.1 and 1 m*M*, respectively. Thus, the ITC experiments were performed under conditions in which the *C* value ($K_b \times Mt$, where K_b and Mt represent the binding constant and the enzyme concentration, respectively) was greater than 1.

Table 1
Data-collection statistics and refinement parameters.

Values in parentheses are for the highest resolution shell.

Complex	Citrate	Initiation	Intermediate	End	ADP (soaked)	ADP (cocrystallized)	CoA	ADP and pantothenate
Space group	$P3_121$	$P3_121$	$P3_121$	$P3_121$	$P3_121$	$P3_121$	$P3_121$	$P3_121$
Unit-cell parameters (Å)	a = 103.51, c = 90.66	a = 102.94, c = 91.23	a = 104.22, c = 90.64	a = 104.09, c = 90.44	a = 104.13, c = 90.25	a = 104.17, c = 90.54	a = 103.84, c = 89.60	a = 104.19, c = 90.30
V_M (Å^3 Da^{-1})	3.99	3.98	4.05	4.03	3.86	3.88	3.81	3.87
Solvent content (%)	69.22	69.08	69.64	69.50	68.15	68.28	67.74	68.21
No. of subunits in ASU	1	1	1	1	1	1	1	1
Resolution (Å)	30.0–2.65	42.0–2.50	35.0–2.80	40.0–2.50	40.0–2.75	40.0–2.80	45.0–2.50	40.0–2.70
Highest shell (Å)	2.74–2.65	2.59–2.50	2.90–2.80	2.59–2.50	2.85–2.75	2.90–2.80	2.59–2.50	2.80–2.70
No. of measured reflections	160286	139393	101592	104452	144339	130743	190303	156913
No. of unique reflections	16603 (1567)	19556 (1835)	14172 (1343)	19980 (1991)	15061 (1463)	14360 (1414)	19644 (1941)	15934 (1554)
Completeness (%)	99.2 (95.5)	99.2 (95.6)	98.4 (94.2)	99.8 (99.9)	100.0 (99.8)	100.0 (99.7)	99.8 (99.0)	100 (100)
R_{merge}†	10.9 (46.9)	5.8 (57.2)	9.9 (59.4)	7.8 (57.1)	7.7 (54.3)	7.9 (52.6)	8.8 (58.4)	7.4 (55.5)
$I/\sigma(I)$	16.9 (2.2)	31.5 (2.4)	16.9 (2.6)	21.9 (3.2)	30.5 (3.1)	31.4 (5.3)	22.5 (2.6)	34.2 (4.7)
Multiplicity	9.7 (2.4)	7.1 (4.2)	7.2 (5.3)	5.3 (5.1)	9.6 (5.5)	9.1 (9.0)	9.7 (6.3)	9.8 (9.8)
Refinement and model statistics								
No. of reflections	16552	19528	14133	19963	15041	14337	19618	15912
R factor (%)	20.3	22.1	21.4	19.8	20.7	20.7	20.6	20.3
R_{free}‡ (%)	24.5	25.7	25.3	23.6	23.8	23.5	24.0	23.3
No. of atoms in ASU								
Protein	2473	2495	2485	2487	2484	2480	2481	2480
Ligand/ion	94	121	120	117	63	57	147	93
Water	186	136	103	224	150	132	190	184
R.m.s. deviations from ideal								
Bond lengths (Å)	0.007	0.006	0.007	0.006	0.009	0.009	0.007	0.010
Bond angles (°)	1.3	1.3	1.6	1.4	1.6	1.5	1.5	1.6
Dihedral angles (°)	23.5	23.1	23.0	22.7	23.7	24.1	24.0	23.6
Improper angles (°)	0.8	1.8	1.7	1.7	1.8	1.7	2.4	2.2
Ramachandran plot statistics§								
Most favoured region (%)	89.4	91.2	90.1	90.1	87.5	88.3	89.7	89.4
Additionally allowed region (%)	9.5	7.3	7.7	8.4	10.6	10.3	9.2	9.2
Genereously allowed region (%)	1.1	1.5	1.8	1.5	1.5	1.5	1.1	1.5
Disallowed region (%)	0	0	0.4	0.0	0.4	0	0.0	0.0

† $R_{merge} = \sum_{hkl}\sum_i |I_i(hkl) - \langle I(hkl)\rangle| / \sum_{hkl}\sum_i I_i(hkl)$, where $I_i(hkl)$ is the ith intensity measurement of a reflection, $\langle I(hkl)\rangle$ is the average intensity value of that reflection and the summation is over all measurements. ‡ 5% of the reflections were used for the R_{free} calculations. § Calculated for nonglycine and nonproline residues using *PROCHECK*.

Titrations were performed by the stepwise addition of small volumes (4 µl) of ligand (CoA) solution from the stirred syringe (300 rev min^{-1}) into the sample cell. A time interval of 180 s was used between successive injections. Values of the change in enthalpy (ΔH_b), K_b and n for the titration were determined by nonlinear least-squares fitting of the data using *Origin* 7.0 software. The change in entropy (ΔS) was obtained using the equation $\Delta G_b = \Delta H_b - T\Delta S$, where $\Delta G_b = -RT\ln K_b$; R and T represent the gas constant and the absolute temperature (in K), respectively.

2.4. Kinase activity of *Mt*PanK and *Ec*PanK

To determine the kinase activity, purified CoA-free *Mt*PanK and *Ec*PanK were dialyzed for 24 h against 0.1 *M* citrate buffer containing 0.2 *M* NaCl and 10% glycerol with pH ranging from 5.6 to 6.2. The dialyzed protein (30 µ*M*) at different pH values was incubated overnight at 310 K with 0.5 m*M* ATP, 0.4 µ*M* D-pantothenate, 8 µ*M* D-[1-^{14}C]-pantothenate (specific activity 50 mCi mmol^{-1}) and 2.5 m*M* $MgCl_2$ in a reaction volume of 50 µl. To determine the amount of phosphopantothenate formed by the enzyme, the reaction was stopped by heating the reaction mixture for 10 min at 353 K and immediately loading the sample onto a DE81 filter. The filter was air-dried and washed three times with 95% ethanol + 1% acetic acid solution. Counts for each filter were measured using a scintillation counter upon immersing the air-dried filter into the scintillation fluid. The experiment was repeated with two different batches of protein and an average activity profile was generated.

2.5. Determination of kinetic parameters of *Ec*PanK and *Mt*PanK using ITC

To determine the kinetic parameters for ATP hydrolysis, *Ec*PanK and *Mt*PanK were dialysed for 24 h against 0.1 *M* citrate buffer pH 6.0 containing 0.2 *M* NaCl and 10% glycerol. The dialyzed protein was incubated with 1 m*M* pantothenate for half an hour on an end-on rocker at 293 K. The reaction was started by injection of a small volume (8 µl) of ATP (12.5 m*M*) solution into the sample cell loaded with 1 µ*M* enzyme saturated with pantothenate. Multiple injections were given to ascertain the maximum velocity of the enzymatic reaction. A gap of 150 s was left between subsequent injections. K_m for ATP was determined by fitting the reaction rate values obtained to a rectangular hyperbola. k_{cat} was determined using the formula

$$k_{\rm cat} = \frac{\Delta P_{\rm max}}{\Delta H \times V \times [\rm Enzyme]},$$

where $\Delta P_{\rm max}$ is the maximum power, V is the volume of the ITC cell, ΔH is the enthalpy change of the reaction and [Enzyme] is the enzyme concentration in the ITC cell. The experiment was repeated using 0.1 μM protein samples dialyzed against 0.1 M Tris–HCl buffer pH 8.0 containing 0.2 M NaCl and 10% glycerol.

2.6. Crystallization and data collection

Crystals of CoA-free *Mt*PanK suitable for diffraction study were grown by the hanging-drop vapour-diffusion method. Drops prepared by mixing 2–3 µl protein solution (4.5–6 mg ml^{-1}) with 0.5 µl precipitant solution consisting of 1.4–1.8 M trisodium citrate (in water), 0.05–0.1 M sodium acetate (in water) and 7.5–10% glycerol at pH 6.5 were equilibrated against 400 µl precipitant solution. The initiation complex was prepared by adding 1 µl of a cocktail consisting of 1 µl precipitant solution, 1 µl 0.5 M AMPPCP (in water), 1 µl 0.5 M calcium pantothenate (in water), 0.4 µl 0.5 M magnesium chloride (in water) and 1 µl 50% ethylene glycol (in protein buffer) to the crystallization drop and soaking native crystals in the cocktail for more than 24 h prior to data collection. The intermediate complex was obtained by dipping the crystal into a solution consisting of 0.5 M magnesium chloride and 1 M ATP and immediately flash-freezing it within 15 s for data collection. The end complex was prepared in a similar manner with a cocktail containing 1.25 µl 0.5 M ATP (in protein buffer), 1 µl 0.5 M calcium pantothenate (in protein buffer) and 1 µl 0.5 M magnesium chloride (in protein buffer), 0.75 µl of which was added to the crystallization drop. A similar protocol was used to soak *Mt*PanK crystals with ADP and pantothenate, ADP and CoA. An attempt was also made to cocrystallize *Mt*PanK with ATPγS by adding a solution of the ligand in citrate buffer to the protein solution dropwise until a concentration of 8 mM was reached and then incubating the solution overnight at 277 K before setting up crystallization. In the event, an ADP complex was obtained. Presumably, ATPγS was hydrolyzed in the citrate buffer. A similar hydrolysis has been reported previously during the preparation of a nucleotide complex of 5-methylthioribose kinase from *Arabidopsis thaliana* (Ku *et al.*, 2007). All the ligands used in the study were obtained from Sigma–Aldrich.

X-ray diffraction data were collected using a MAR 345 image plate mounted on a Rigaku RU200 rotating-anode X-ray generator with an oscillation angle of 1° using crystals flash-frozen (100 K) in a liquid-nitrogen stream produced by an Oxford Cryosystem. The recorded images were processed and scaled using *DENZO* and *SCALEPACK* from the *HKL* package and the intensity data were truncated to amplitudes using *TRUNCATE* from the *CCP*4 suite (Otwinowski & Minor, 1997; Collaborative Computational Project, Number 4, 1994). Refinement parameters, together with data-collection statistics, are given in Table 1.

2.7. Structure solution, refinement and validation

The structures were solved by molecular replacement using *AMoRe* (Navaza, 1994) with the *Mt*PanK structure (PDB code 2gev) as the search model. Refinement for all structures was performed using *CNS* v.1.1 (Brünger *et al.*, 1998). The struc-

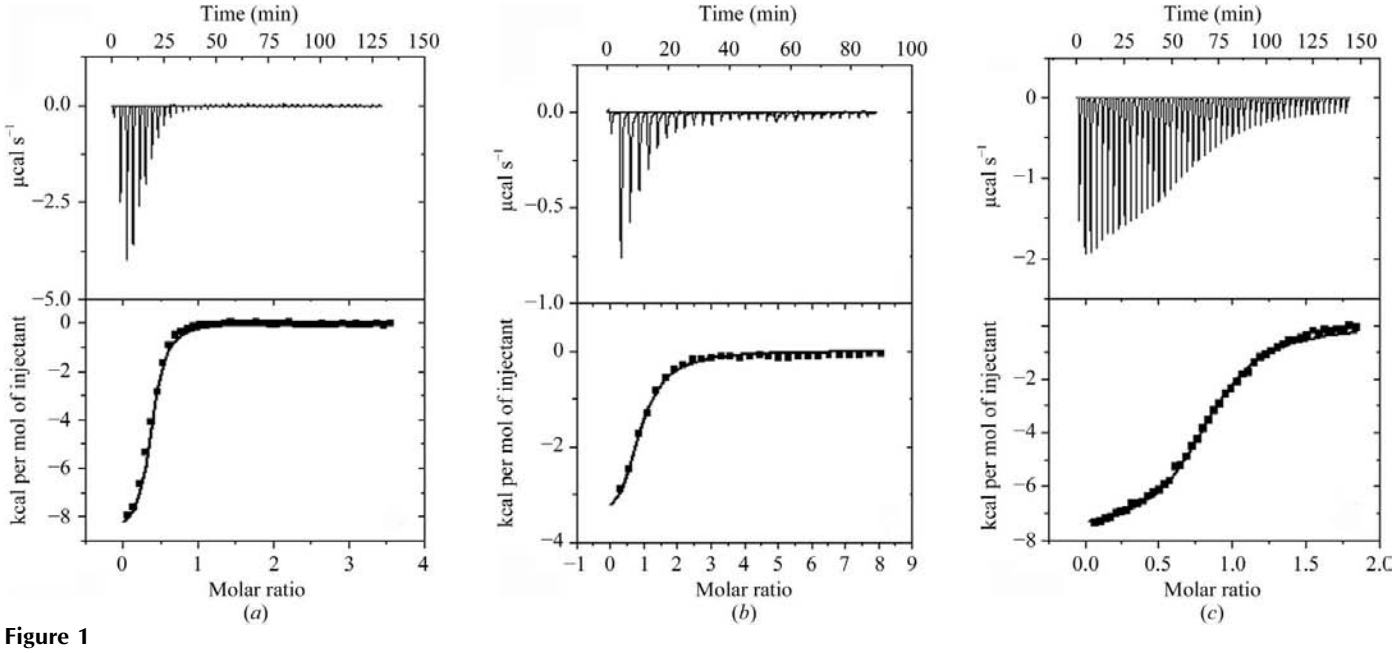

Figure 1
Isothermal titration calorimetry of *Mt*PanK and *Ec*PanK with CoA. The upper panel in each graph shows the heat change elicited upon successive injections of CoA into *Mt*PanK and *Ec*PanK. The first injection of each titration was performed with 2 µl CoA to minimize the contribution of any artefact associated with the loading of the syringe with the ligand. The lower panel in each case shows the binding isotherm as a function of the molar ratio of ligand to enzyme. In each case a theoretical curve was fitted to the integrated data using a single-site model. (*a*) *Mt*PanK in Tris–HCl buffer as purified; (*b*) *Mt*PanK dialysed against citrate buffer; (*c*) *Ec*PanK in Tris–HCl buffer as purified. See text for details. 1 cal = 4.186 J.

Table 2
Thermodynamic parameters for the binding of CoA to *Mt*PanK and *Ec*PanK (see text for details).

	T (K)	n	K_b (M^{-1})	ΔH_b (kJ M^{-1})	ΔG_b (kJ M^{-1})	ΔS (J M^{-1} K^{-1})
*Mt*PanK	293	0.35	2.12×10^5	−35.8	−29.8	−20.0
*Mt*PanK dialyzed against citrate buffer	293	0.82	1.50×10^5	−17.7	−29.0	+39.0
*Ec*PanK	293	0.84	1.58×10^5	−32.2	−29.1	−10.3

Table 3
Kinetic parameters of ATP hydrolysis by *Mt*PanK and *Ec*PanK (see text for details).

	Buffer	K_m (mM)	k_{cat} (s^{-1})	k_{cat}/K_m (s^{-1} mM^{-1})
*Mt*PanK	Citrate pH 6.0	0.616 ± 0.043	0.052 ± 0.001	0.08
	Tris–HCl pH 8.0	0.151 ± 0.012	0.411 ± 0.016	2.72
*Ec*PanK	Citrate pH 6.0	0.406 ± 0.021	0.071 ± 0.001	0.17
	Tris–HCl pH 8.0	0.115 ± 0.015	1.140 ± 0.042	9.91

tures were initially subjected to rigid-body refinement followed by positional refinement and simulated annealing. Electron-density maps with Fourier coefficients $2F_o - F_c$ and $F_o - F_c$ were calculated at this stage. These maps permitted the initial unambiguous positioning of the ligands. Iterative model building and refinement was carried out until convergence of R and R_{free}. Model building was carried out using the interactive graphics program *Coot* (Emsley & Cowtan, 2004). In all structures water molecules were built into the electron-density maps where the peaks were visible at contours of at least 3.0σ in $F_o - F_c$ and 1σ in $2F_o - F_c$ electron-density maps. The topology and parameter files for various ligands were generated using the *PRODRG* server (Schüttelkopf & van Aalten, 2004). The models were validated using *PROCHECK* and *MOLPROBITY* (Laskowski *et al.*, 1993; Davis *et al.*, 2007). Secondary structure was assigned using *DSSP* (Kabsch & Sander, 1983). Structural superpositions were made using *ALIGN* (Cohen, 1997). Interatomic distances were calculated using *CONTACT* from the *CCP*4 program suite (Collaborative Computational Project, Number 4, 1994). All figures for molecular representation were prepared using *PyMOL* (DeLano, 2002).

3. Results

3.1. Energetics of CoA binding, removal of bound CoA and kinase activity of *Mt*PanK

During purification, *Mt*PanK elutes substantially as a complex with CoA, even when the coenzyme was not externally added to the medium. In any case, it is the CoA-bound enzyme that crystallizes, as demonstrated by X-ray analysis (Das *et al.*, 2006). Presumably, recombinant *Mt*PanK sequesters intracellular CoA during expression and purifies in a CoA-bound form. It was necessary to remove the coenzyme from the protein in order to explore its interactions with other ligands. This could not be achieved through repeated dialysis of the protein sample against the buffer used for purification. No such difficulty was reported in the case of *Ec*PanK. This prompted an isothermal titration calorimetric study of the enzyme from the two sources (Fig. 1). The sample of *Ec*PanK used in this study was cloned, expressed and purified in the same way as was *Mt*PanK (Das *et al.*, 2005). The results clearly showed the affinity of CoA for *Mt*PanK to be higher than that for *Ec*PanK. Furthermore, nearly 84% of the population in *Ec*PanK (as isolated) has empty CoA-binding sites, while this is only the case for about 35% of the population in *Mt*PanK (Table 2).

As was performed in the case of phosphopantetheine adenyltransferase, we sought to remove CoA from *Mt*PanK through extensive dialysis of the purified sample against citrate buffer pH 5.6 (Geerlof *et al.*, 1999). Subsequent ITC measurements confirmed substantial removal of CoA (Table 2). The proportion of CoA-free enzyme was now comparable to that in the sample of *Ec*PanK. Interestingly, the enthalpy of interaction with CoA of *Mt*PanK samples dialysed against citrate buffer was lower than that of the original samples. Furthermore, the change in entropy was now positive. The explanation for this anomaly became apparent when the crystal structure of the sample was examined. In the structure, two citrate ions are strongly bound at the CoA-binding site (see later). Thus, the measured enthalpy is the difference between the enthalpies of binding to CoA and citrate. The same is also true in the case of the change in entropy.

The kinase activity of *Mt*PanK was measured in a protein solution identical to that used for crystallization, employing radioactive pantothenate at intervals of 0.2 pH units in the pH range 5.6–6.2, which roughly corresponds to the range of pH in the crystallization drops (Fig. 2). Experiments conducted on recombinant *Ec*PanK under identical conditions yielded similar results but with higher counts. The rates of reaction catalyzed by *Mt*PanK and *Ec*PanK measured at pH 6.0 in the same buffer are given in Table 3. They have similar reaction profiles (Fig. 3), but the rate is uniformly higher for *Ec*PanK.

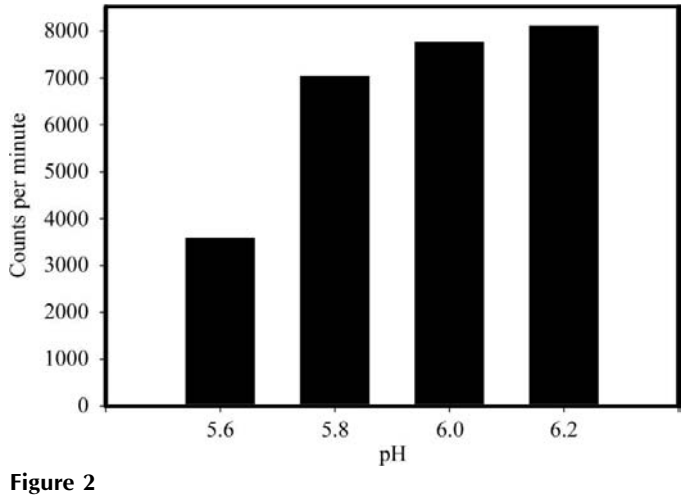

Figure 2
Kinase activity profile for *Mt*PanK in 0.1 *M* citrate buffer. See text for details.

The K_m and k_{cat} values also show higher catalytic efficiency for *Ec*PanK. The same trend is also maintained at pH 8.0 in 0.1 *M* Tris–HCl buffer. The same buffer at the same pH was used previously for the crystallization of the three complexes of *Ec*PanK and the CoA complex of *Mt*PanK. Thus, it was ensured that the measurements of activity on *Mt*PanK and *Ec*PanK were carried out under the same conditions as those used for crystallization.

3.2. Reliability, significance and overall features

Eight crystal structures are considered here. The native crystals contained bound citrate ions from the buffer. The remaining seven structures are those of complexes prepared by soaking except for one case. Three of them represent important stages in the reaction pathway. One of them contains AMPPCP and pantothenate and another contains ADP and phosphopantothenate in the active site. The electron density in the binding site of the third is consistent with the presence of ATP and ADP molecules with 50% occupancy. Another complex contains ADP and pantothenate and yet another CoA. Complexes with ADP alone as the ligand were prepared by soaking as well as by cocrystallization. All of them belong to the same space group with comparable unit-cell parameters and one subunit in the asymmetric unit. The physiological dimer, identified on the basis of homology to *Ec*PanK, is generated by a crystallographic dyad. The structures are isomorphous among themselves, with r.m.s. deviations in C^{α} positions between pairs of structures in the range 0.23–0.41 Å. The number of C^{α} positions superposed is 307 in all cases.

The eight structures presented here are isomorphous to form II of the *Mt*PanK–CoA complex reported previously (Das *et al.*, 2006). The structure of the latter was derived from crystals of a preformed complex grown from 0.1 *M* Tris–HCl buffer pH 8.0. The *Mt*PanK–CoA complex reported here was prepared by soaking the native crystals in a CoA solution in citrate buffer pH 5.6. The protein molecules in the two structures superpose with an r.m.s. deviation in C^{α} positions of 0.28 Å for 307 residues. Likewise, the ligand atoms superpose

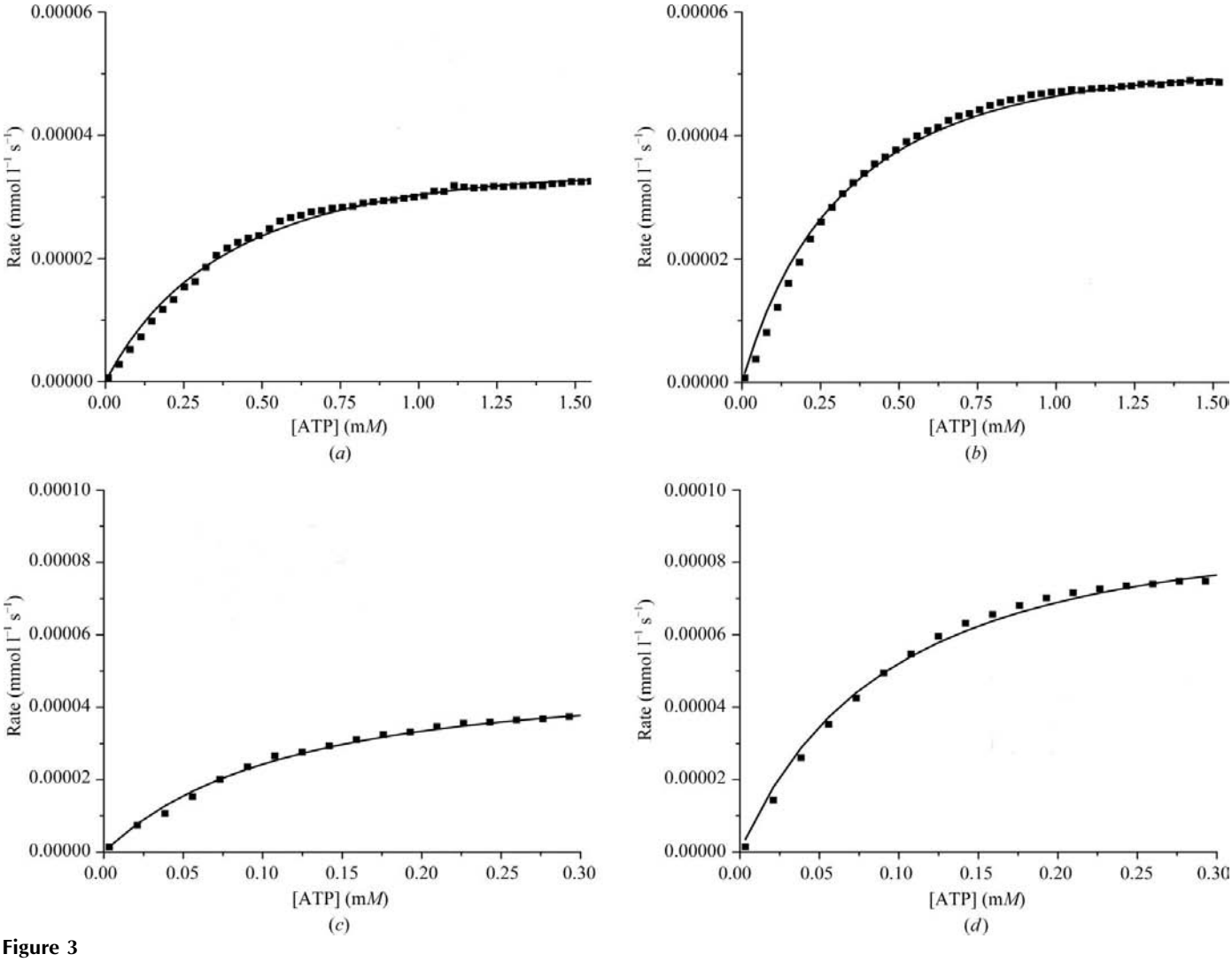

Figure 3
Kinetic parameters for ATP hydrolysis by *Mt*PanK and *Ec*PanK. (*a*) and (*b*) are reaction rate profiles for *Mt*PanK and *Ec*PanK, respectively, in 0.1 *M* citrate buffer pH 6.0; (*c*) and (*d*) are reaction rate profiles for *Mt*PanK and *Ec*PanK, respectively, in 0.1 *M* Tris–HCl pH 8.0. See text for details.

with an r.m.s. deviation of 0.77 Å for 48 atoms. Thus, cocrystallization and soaking lead to the same results. The structure is also unaffected by the composition of the buffer solution and variation of pH. Crystals of the ADP complex prepared by soaking as well as cocrystallization lead to identical results, further indicating the reliability and significance of the nucleotide complexes prepared by soaking.

The first five residues in all reported structures are disordered. In addition, the side chains of residues 83 and 84 in the structure of the native enzyme, residue 83 in the CoA-soaked structure and in the end complex and residue 86 in the intermediate complex of *Mt*PanK have no electron density. Except for these few residues, the structures, including the ligands (Fig. 4), have well defined electron density. The 312-residue polypeptide chain in each subunit adopts a mononucleotide-binding fold with a seven-stranded mixed β-sheet (S1–S3 and S6–S9) surrounded by helices. A small two-stranded sheet (S4, S5) also exists in the structure (Fig. 5). The helices and strands are interconnected by elaborated loops.

The formation of the dimer involves the burial of nearly 4000 Å^2 of surface area belonging to the two subunits, of

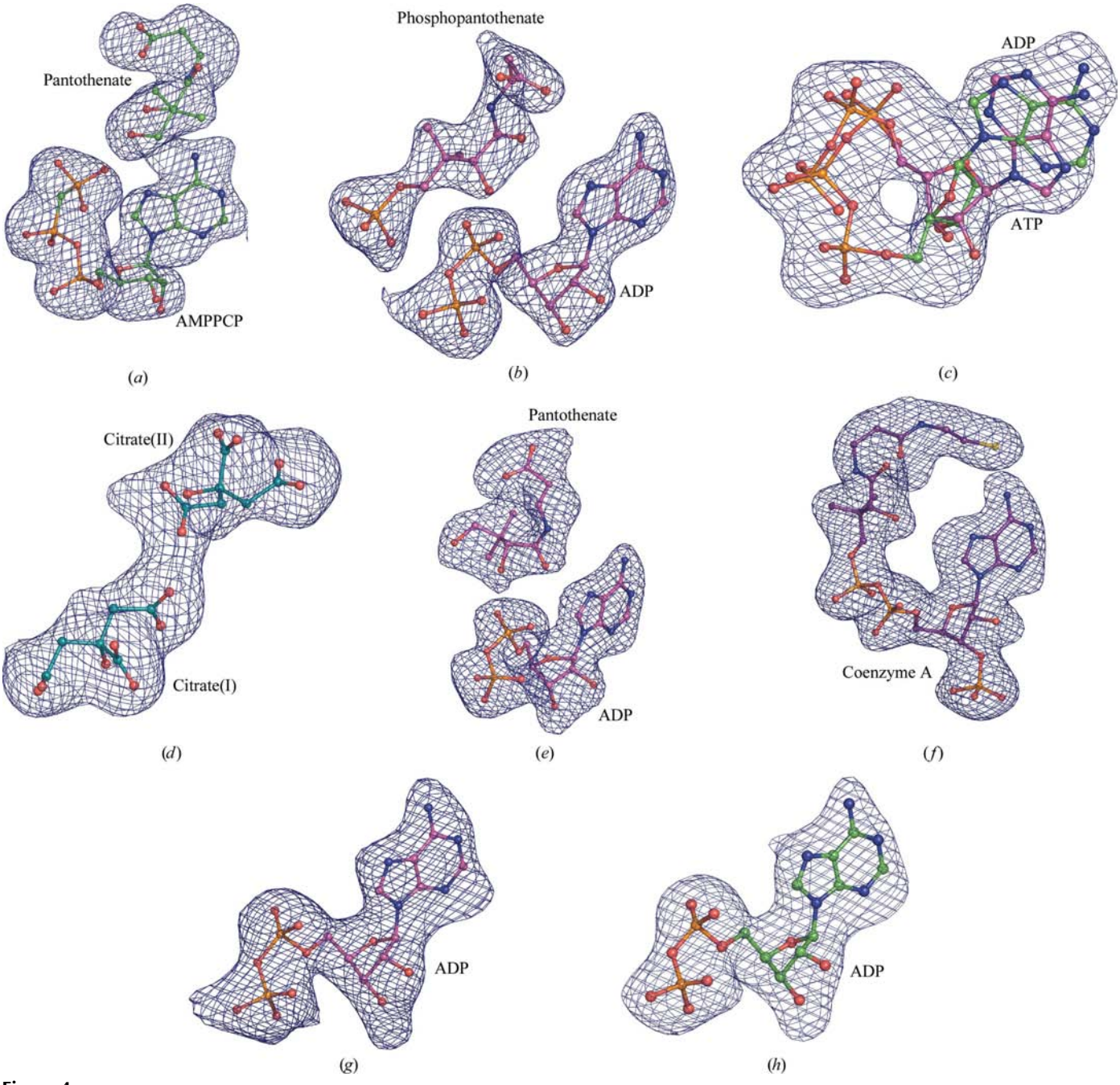

Figure 4
Simulated-annealing OMIT maps with Fourier coefficients $F_o - F_c$ contoured at 3σ for ligands bound to *Mt*PanK in (*a*) the initiation complex, (*b*) the end complex, (*c*) the intermediate complex, (*d*) the citrate complex, (*e*) the ADP and pantothenate complex, (*f*) the CoA complex, (*g*) the soaked ADP complex and (*h*) the cocrystallized ADP complex.

which nearly 3000 Å^2 is nonpolar. The intersubunit interface is made up of nearly 50 residues belonging to helices, loops and the terminal regions. In particular, helix H4 and its partner from the other subunit form a coiled coil. The residues involved are nearly the same in the structures of *Mt*PanK and *Ec*PanK (Das *et al.*, 2006). However, a comparison of the structures provides evidence for some structural plasticity at the interface within species and across species. A comparison of PanK sequences from different bacteria has also shown poor conservation of amino acids in this region. This interface region therefore carries a strong signature of the differences between different PanKs (Das *et al.*, 2006).

3.3. Protein–ligand interactions

CoA, which is an inhibitor, and the other ligands, most of which form part of the reaction cycle, share a substantially common binding site. The protein–ligand interactions in the *Mt*PanK–CoA complex reported here are the same as those in the complex derived from crystals grown at higher pH (Das *et al.*, 2006). In terms of change in the accessible surface area of residues on ligand binding and hydrogen bonding, about 35 residues are involved in ligand binding in the initiation, intermediate and end complexes. Of these, all but seven participate in CoA binding. The locations of the ligands in the two complexes, that with ADP and pantothenate and the (native) structure in which the binding site is occupied by two citrate ions, are illustrated in Fig. 6. The hydrogen bonds involved in protein–ligand interactions in these complexes are given in Table 4.

In the initiation complex as well as the end complex, the phosphate groups of the nucleotide interact with the P-loop (Figs. 6*a* and 6*b*). However, the locations of the nucleoside component are somewhat different in the two structures. The difference is caused by a lateral shift and a conformational change. In both cases the nucleoside is in contact with (<4 Å) Ser104, His179, Arg238 and Met242. That in AMPPCP is additionally in contact with Arg108, while ADP is in contact with Ala246, Phe247 and Phe254. The difference in the location and the conformations of the nucleosides is such that the phosphate groups attached to them point in opposite directions. Consequently, the α-phosphate group in ADP in the end complex is close to the location of the γ-phosphate of AMPPCP in the initiation complex. The locations of the β-phosphate are close to each other when the structures are superposed. ADP binds at the same location in its complex with *Mt*PanK as it does in the end complex, irrespective of the method of preparation of the former (soaking or cocrystallization). The same is true regarding its location in the ternary complex that also involves pantothenate (Fig. 6*d*). Thus, that observed in the end complex is the natural location of ADP in *Mt*PanK. The r.m.s. deviations in atomic positions in ADP among the three complexes vary between 0.19 and 0.79 Å for 27 atoms.

Unlike ATP analogues in most protein complexes, AMPPCP in the initiation complex has a closed conformation similar to that of free ATP in its crystal structure (Kennard *et al.*, 1971). The closed conformation involves the proximity of the negatively charged γ-phosphate and the base carrying positive charges. In the absence of γ-phosphate, the closed conformation does not offer any energetic advantage to ADP. On the other hand, the somewhat extended conformation of the type formed in the end complex permits an extensive set of protein–ADP interactions. In any case, a closed conformation of ADP of the type exhibited by AMPPCP is not sterically compatible with its position in the end complex. Thus, the difference between the locations of AMPPCP and ADP in the initiation and end complexes could have resulted from a subtle balance between intramolecular and intermolecular interactions.

The binding region of pantothenate in the initiation complex is entirely different from that of phosphopantothenate in the end complex. The former is substantially hydrophobic, whereas several hydrogen bonds are involved in the binding of phosphopantothenate to the enzyme (Table 4). Only two residues, Tyr235 and Asn277, are common to both binding sites (Figs. 6*a* and 6*b*). Phosphopantothenate in the end complex and pantothenate in the ternary complex involving ADP bind at the same location, although for reasons explained later there are differences in the *Mt*PanK–pantothenate interactions.

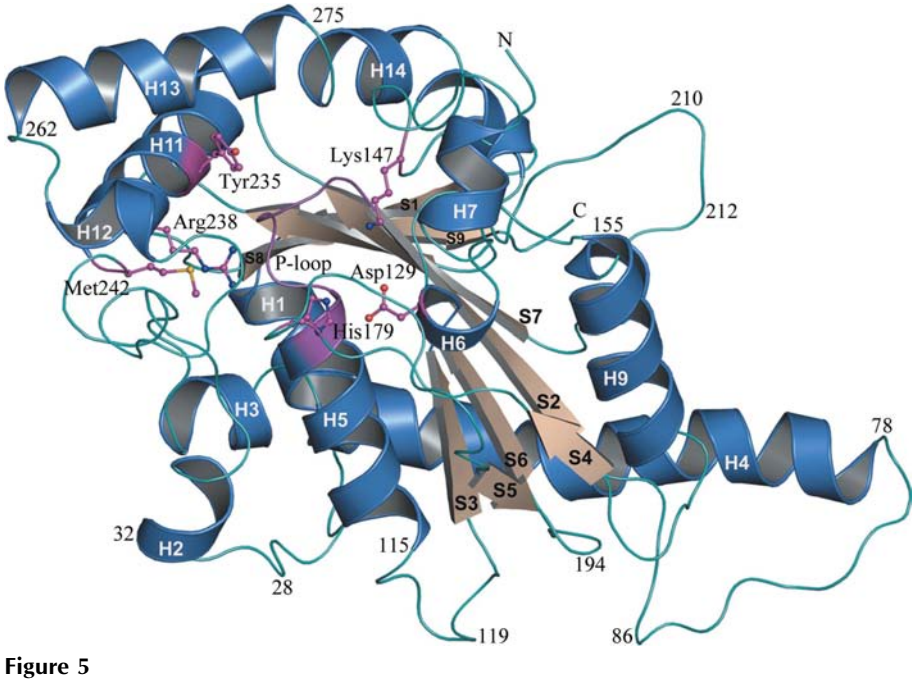

Figure 5
Overall structure of *Mt*PanK. The key residues that make up the ligand-binding pocket are shown in ball-and-stick representation.

Table 4
Atoms involved in protein–ligand hydrogen bonds in the initiation, intermediate and end complexes of *Mt*PanK.

The hydrogen bonds formed by ADP, pantothenate and citrate in the other complexes by and large form subsets of those listed here. Additional hydrogen bonds in these complexes are separately indicated in the text or figures. For the numbering scheme of ligands, refer to Figs. 6 and 7.

		Initiation complex		Intermediate complex		End complex	
Residue No.	Atom name	AMPPCP	Pantothenate	ATP	ADP	ADP	Phosphopantothenate
Ala100	N	O3B	—	O3B	O3A	O1B	—
				O2B	O1A	O1A	
					O2A		
Val101	N	O2B	—	O2B	O1B	O2B	—
						O1B	
Gly102	N	O2B	—	O2B	O1B	O2B	—
						O1B	
Lys103	N	O2B	—	—	—	O2B	—
						O3B	
	NZ	—	—	O1B	O2B	O2B	—
				O2G	O1A	O3A	
Ser104	OG	O1B	—	O1B	O2B	O3B	—
	N	O1B	—	O1B	O2B	O3B	—
		O1A					
Thr105	OG1	O2A	—	O1A	—	—	—
		O1A					
	N	O1A	—	O1A	—	—	—
Arg108	NH1	O2′	—	O3′	O3′	—	—
	NH2	O5′	—	O1A	—	—	—
Thr128	OG1	—	—	—	—	—	O8
Asp129	OD2	—	—	—	—	—	—
	N						O6
Lys147	O	—	—	—	—	—	—
Tyr153	OH	—	—	—	—	—	O8
							O2
His179	NE2	—	—	—	—	—	O5′
							O6′
Leu203	N	—	—	—	—	—	O7
Tyr235	OH	—	OXT	—	—	—	O
							OXT
Arg238	NE	—	O2	—	—	—	—
	NH1	—	—	—	—	O1B	—
						O1A	
	NH2	O2G	O2	O1G	O2A	O1A	—
				O3B	O5′		
Asn277	ND2	—	—	—	—	—	OXT
	OD1	—	—	—	—	—	OXT

Thus, the locations observed in the two complexes appear to be the preferred location of pantothenate in the presence of bound ADP.

Interestingly, the guanidinium group of Arg238 bridges the γ-phosphate group of AMPPCP and the terminal hydroxyl O atom of pantothenate in the initiation complex (Fig. 6*a*). In the end complex, ADP and phosphopantothenate are interconnected by a hydrogen bond formed between the O atom of the α-phosphate of ADP and the O5′ hydroxyl of phosphopantothenate (Fig. 6*b*). Thus, the two ligands are interconnected in both complexes. Superposition of the two complexes using C^{α} positions clearly indicates that the binding site of ADP in the end complex and that of pantothenate in the initiation complex overlap. The binding of the two ligands at the respective binding sites would result in a clash between the central amide group of pantothenate and the base of ADP. Similarly, when phosphopantothenate is placed in its respective binding site in the initiation complex, it is seen that the transferred phosphate group and the terminal carboxylate of phosphopantothenate clash with the side chains of Thr128, Asp129 and Asn277.

The location of the citrate ions in the apo structure are also interesting (Fig. 6*c*). One of them interacts with the P-loop and occupies the region occupied by the phosphate groups in the nucleotide-bound enzyme. The location of the other ion roughly corresponds to that of phosphopantothenate in the end complex. Thus, the citrate ions effectively block the active site of the enzyme. As mentioned earlier, this explains the anomalously low magnitude of the change in enthalpy when CoA interacts with the enzyme in the citrate buffer.

3.4. Change in ligand positions in the complexes

The protein–ligand interactions in the different complexes described above are consistent with the sequence of events outlined below and illustrated in Fig. 7. Upon phosphorylation, pantothenate rotates around a pivotal region roughly defined by its own carboxyl end, Tyr235 OH and the side-chain amide group of Asn277. The movement involved in this rotation is substantial: the hydroxyl O atom of pantothenate moves by as much as 10 Å. Two factors appear to cause this rotation. Upon hydrolysis of ATP to ADP, the adenine base moves into the pantothenate-binding pocket, resulting in a steric clash with the pantothenate amide group, which can only be relieved by a movement of phosphopantothenate. This movement is further facilitated by the formation of several hydrogen bonds between the transferred phosphate group and the protein atoms in the new position.

As indicated earlier, although pantothenate and phosphopantothenate bind at the same location in their respective ternary complexes involving ADP, differences exist in the detail. The two structures provide an explanation of the differences in terms of movements caused by phosphorylation. In the pantothenate complex, the side chain of Asp129 makes a hydrogen bond to the side chain of His179 (Fig. 6*d*). On phosphorylation, the aspartyl side chain is pushed away and the phosphate group establishes hydrogen bonds to Thr128 O, Asp129 N and Tyr153 OH. The hydrogen bond of His179 to Asp129 is broken and consequently the imidazole ring moves and rotates by 180° to form hydrogen bonds to two central O atoms of phosphopantothenate (Fig. 6*b*). These new interactions result in the straightening of the pantothenate moiety and its slight relocation.

3.5. Comparison with protein–ligand interactions in *Ec*PanK

The interactions of CoA with *Mt*PanK and *Ec*PanK, two enzymes which have a sequence identity of 52%, are very similar, except that the former appears to be somewhat stronger in terms of surface area buried and the number of hydrogen bonds. The CoA complexes of the two enzymes superpose with r.m.s. deviations of 0.85 Å for 282 C^{α} positions. Unlike in the case of CoA, the interactions of ATP, ADP and pantothenate with *Ec*PanK are substantially different from those with *Mt*PanK. The structure of *Mt*PanK remains the

same on the formation of the initiation and end complexes, involving interactions with ATP and pantothenate in one case and ADP and phosphopantothenate in the other. In contrast, there is a local conformational difference between the CoA-bound enzyme and the enzyme bound to ATP or ADP in the case of *Ec*PanK. Likewise, pantothenate binding causes a local conformational change in the *E. coli* enzyme. The local conformational changes outlined below do not affect the overall molecular structure, but contribute to increasing the r.m.s. deviations in C^{α} positions. The deviation in the AMPPNP complex of *Ec*PanK when superposed on the CoA complex of *Mt*PanK is 2.90 Å for 295 C^{α} positions. The corresponding deviation when the ternary complex of *Ec*PanK with ADP and pantothenate is superposed on the same complex of *Mt*PanK is 2.40 Å for 295 C^{α} positions. The corresponding deviation in C^{α} positions reduces to 2.1 and 1.9 Å, respectively, when the conformationally variable regions of *Ec*PanK (regions 33–48 and 243–268) are not used in calculating the r.m.s. deviations.

The polypeptide stretch involving residues 33–48 (31–46 in the *Mt*PanK numbering scheme) has somewhat different conformations in the complexes of *Ec*PanK with CoA and AMPPNP (Yun *et al.*, 2000). In the CoA complex the 33–37 stretch forms a helical segment followed by two residues in the type III turn (3_{10}-helix) conformation and a loop (Fig. 8*a*). Glu44 is now in the region which binds the base and the sugar and hence blocks the nucleoside-binding pocket. This conformation is therefore referred to as the closed conformation. In the AMPPNP complex, residues 38–42 also form part of the helix (Fig. 8*b*). Thus, the stretch now has a longer 33–42 helix followed by a shorter loop. This change results in Glu44 moving out of the pocket, enabling the nucleoside to enter into it. The conformation could therefore be described as

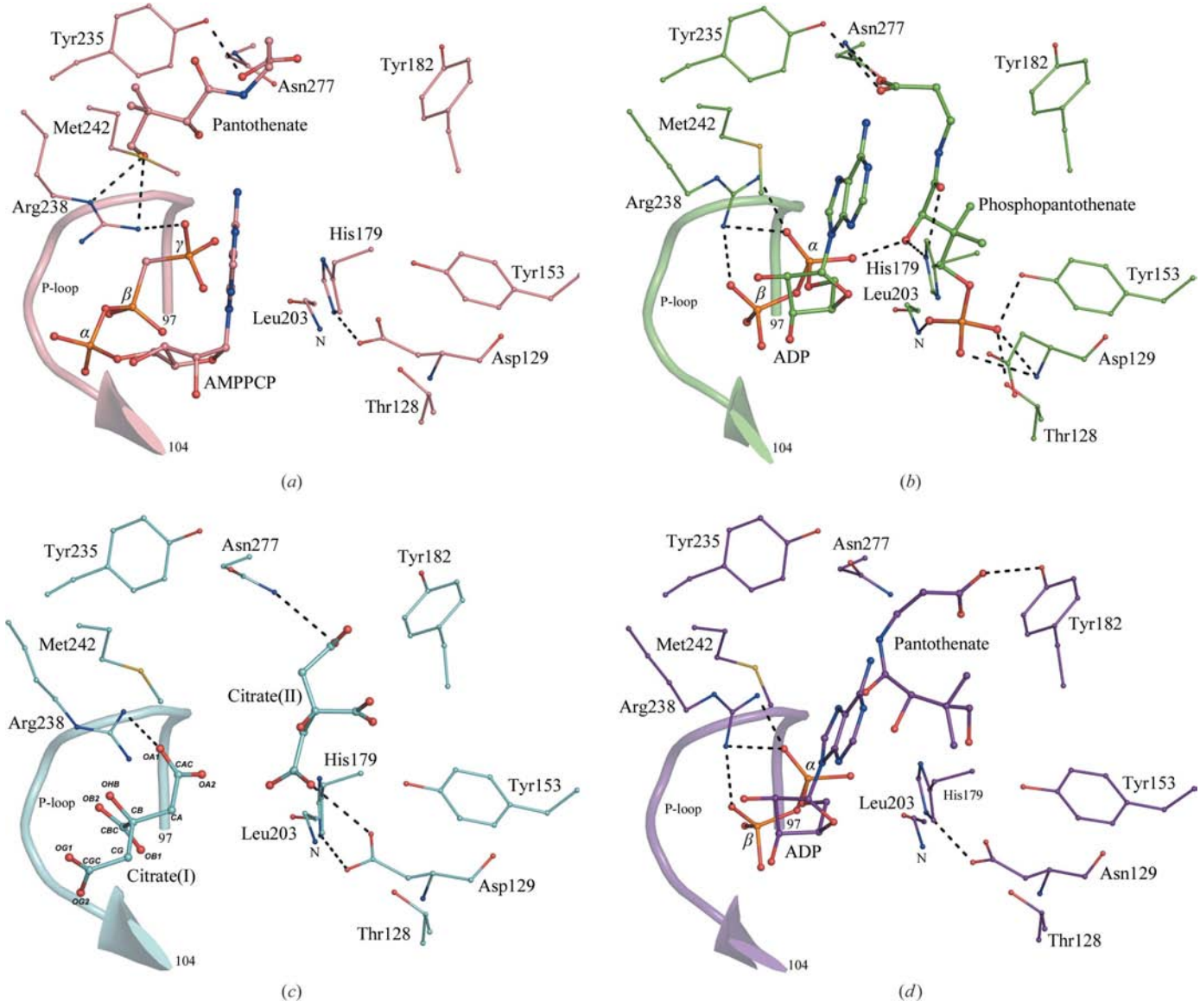

Figure 6
Location and conformation of bound ligands in different *Mt*PanK structures. (*a*) Initiation complex. (*b*) End complex. (*c*) Citrate complex. (*d*) ADP and pantothenate complex.

open. It could well be that the two conformations exist in equilibrium in the native structure and the equilibrium shifts towards the open form in the presence of ATP. ADP also binds to *Ec*PanK in the same way as does AMPPNP (Ivey *et al.*, 2004). The stretch in the complex involving ADP also exhibits the open conformation.

The corresponding stretch in *Mt*PanK has a closed conformation in the CoA complex as well as in the complexes involving AMPPCP and ADP. An intrahelical salt bridge between Arg38 and Asp34 appears to contribute to the stability of the open conformation in *Ec*PanK. Other such interactions include those of Asn43 with Asp45 and Thr103. The residues corresponding to Arg38 and Asn43 are glycines in *Mt*PanK, thus abolishing these interactions. Retention of the closed conformation even in the presence of ATP means that the region corresponding to the nucleoside-binding site in *Ec*PanK is not available for nucleotide binding in *Mt*PanK. AMPPCP therefore has a closed conformation in its complex with *Mt*PanK, which is distinctly different from the extended conformation of AMPPNP in its complex with *Ec*PanK. It also turns out that the overlap between the CoA site and the ATP-binding site is much more extensive in *Mt*PanK than in *Ec*PanK.

In *Ec*PanK in the absence of bound pantothenate, as in the complex with AMPPNP, the side chain of Glu49 is positioned in the substrate-binding pocket and its side-chain carboxylate group occupies the same space as that occupied by the carboxylate end of the pantothenate in the bound form (Fig. 9*a*). In the bound form, the side chain is displaced towards the surface. This displacement is accompanied by a conformational change in the 243–263 stretch (Fig. 9*b*). This involves the incorporation of residues 248–251 into the pre-existing H helix (helix H12 in *Mt*PanK). This conformational change brings together a constellation of conserved residues that forms a hydrophobic lid over the pantothenate-binding pocket (Ivey *et al.*, 2004).

The 243–263 stretch (238–258 in *Mt*PanK) in the CoA complex of *Ec*PanK as well as that of *Mt*PanK has a conformation similar to that in the pantothenate-bound *Ec*PanK structure. This is not surprising as the pantothenate moiety of the coenzyme interacts with this region. However, the conformation of the corresponding region in the intermediate complex (Fig. 9*c*) and the ADP-bound structure of *Mt*PanK (in which the pantothenate-binding region is vacant) resemble the pantothenate-bound structure of *Ec*PanK. The substitution of Glu249 and Gly250 in *Ec*PanK by Thr244 and Thr245 in *Mt*PanK is perhaps largely responsible for the difference between the two in this respect. Both the threonyl residues are involved in interactions which stabilize the helix through intrahelix hydrogen bonds. Also, Thr244 in *Mt*PanK has a shorter side chain than Glu249 in *Ec*PanK and hence is less effective in blocking the pantothenate-binding site. Furthermore, as illustrated in Fig. 6(*c*), in *Mt*PanK the side-chain guanidyl group of the conserved Arg243 forms hydrogen bonds to the side chain of Asp262 and the main-chain carbonyl group of Phe260, contributing to the additional stability of the local conformation of the 238–258 stretch. Asp262 is replaced by a lysine (Lys267) in *Ec*PanK, lending the region more flexibility.

The binding site of pantothenate in *Ec*PanK roughly corresponds to that of phosphopantothenate but not to that of pantothenate in *Mt*PanK. However, interestingly, the phosphorylating end of pantothenate is orientated towards the γ-phosphate of ATP in *Mt*PanK as well as *Ec*PanK, albeit in different ways (Fig. 10). Thus, the pantothenate shares a common region for its carbonyl end in the two cases , but its hydroxyl end is on either side of the γ-phosphate. Also, the location of γ-phosphate is nearly the same in the two cases, despite the

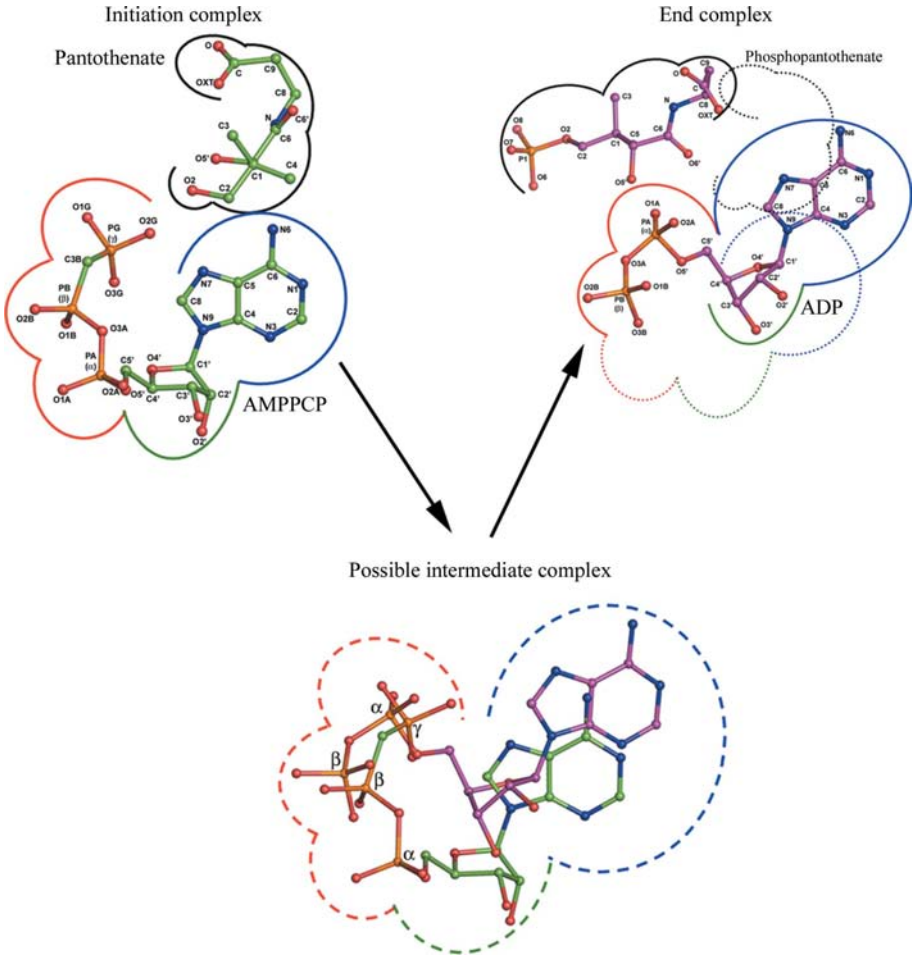

Figure 7
Movement of ligands during enzyme action in *Mt*PanK.

difference in the binding site for ATP in *Mt*PanK and *Ec*PanK. The structure of a complex of *Ec*PanK involving ATP as well as pantothenate is not available. That of a complex of the enzyme involving phosphopantothenate has not yet been reported. However, the location of pantothenate in its complex with *Ec*PanK is such that when it is phosphorylated the product could occupy roughly the site occupied by phosphopantothenate in *Mt*PanK.

Thus, unlike in the case of *Ec*PanK, the binding site in *Mt*PanK is substantially preformed and retains its geometry irrespective of the nature of the ligands. The relocations of the ligands during enzyme action are all within this preformed site. The geometry and the volume of the binding site as calculated using the *CASTp* server (Dundas *et al.*, 2006) is nearly the same at over 1500 Å^3 in the two enzymes when CoA is the ligand. However, changes are induced in the binding site of *Ec*PanK in the presence of ATP, ADP or pantothenate. For instance, the volume of the binding site calculated using the initiation complex of *Mt*PanK is 1655 Å^3, while the volume estimated from the *Ec*PanK–AMPPNP complex is 2097 Å^3. The volume reduces by about 400 Å^3 on AMPPCP binding in the former, while the reduction is close to 1000 Å^3 in the latter. As indicated earlier, the plasticity of the binding site in *Ec*PanK results from changes in the stability of the local conformations consequent to specific amino-acid substitutions in the sequence.

4. Discussion

The work reported here indicates that the geometrical aspects of the enzymatic action of *Mt*PanK could differ from those of the action of the homologous *Ec*PanK. In *Ec*PanK, the locations of the reactants, namely ATP and pantothenate, are nearly the same as those of the appropriate products, namely ADP and phosphopantothenate. However, the reaction catalysed by *Mt*PanK is characterized by substantial changes in their respective locations. This could slow the rate of reaction in *Mt*PanK. On the other hand, *Ec*PanK undergoes local conformational changes during catalysis, whereas *Mt*PanK does not. This could slow the rate in *Ec*PanK. The balance between these two effects could be responsible for the small differences in k_{cat} between the two enzymes. Furthermore, the extended conformation of ATP in the *Ec*PanK–ATP complex results in the burial of a larger surface area than in the *Mt*PanK complex, in which ATP has a folded conformation, thus accounting for the lower K_m value in the reaction involving *Ec*PanK. CoA binds to *Mt*PanK and *Ec*PanK in a similar fashion, but the surface area buried and the number of hydrogen bonds are somewhat higher in the *Mt*PanK complex, thus accounting for the stronger binding of the coenzyme to the *M. tuberculosis* enzyme.

Nucleophilic substitution at phosphorus can in general proceed through an associative or a dissociative pathway (Mildvan, 1997). These two mechanisms represent two limiting cases and enzyme-catalyzed phosphoryl transfer is believed to involve a continuum of mechanisms with both associative and dissociative characteristics (Mildvan, 1997). A rough and ready indication of the nature of the mechanism is provided by the distance between the entering atom and the phosphorus undergoing substitution before the reaction has begun (Mildvan, 1997). When the distance is less than 4.9 Å, the mechanism is likely to have higher associative character; dissociative character dominates when it is greater than 4.9 Å. This distance between the γ-phosphate in AMPPCP and the terminal hydroxyl O atom of the pantothenate in the initiation complex is 4.5 Å in *Mt*PanK. The corresponding distance in *Ec*PanK estimated by superposing the AMPPNP complex and the complex involving ADP and pantothenate is 4.1 Å. These distances need to be treated with caution in view of the medium resolution of the structures, but they are certainly

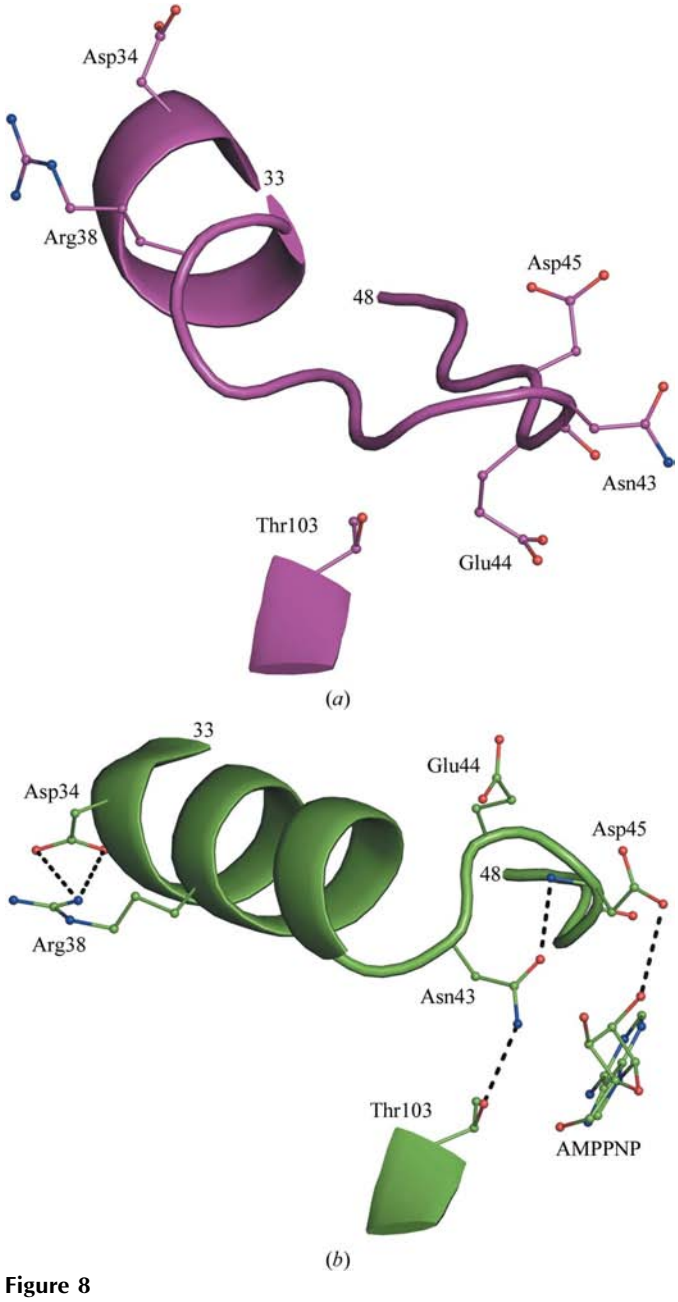

Figure 8
Local conformation of *Ec*PanK when bound to (*a*) CoA and (*b*) AMPPNP.

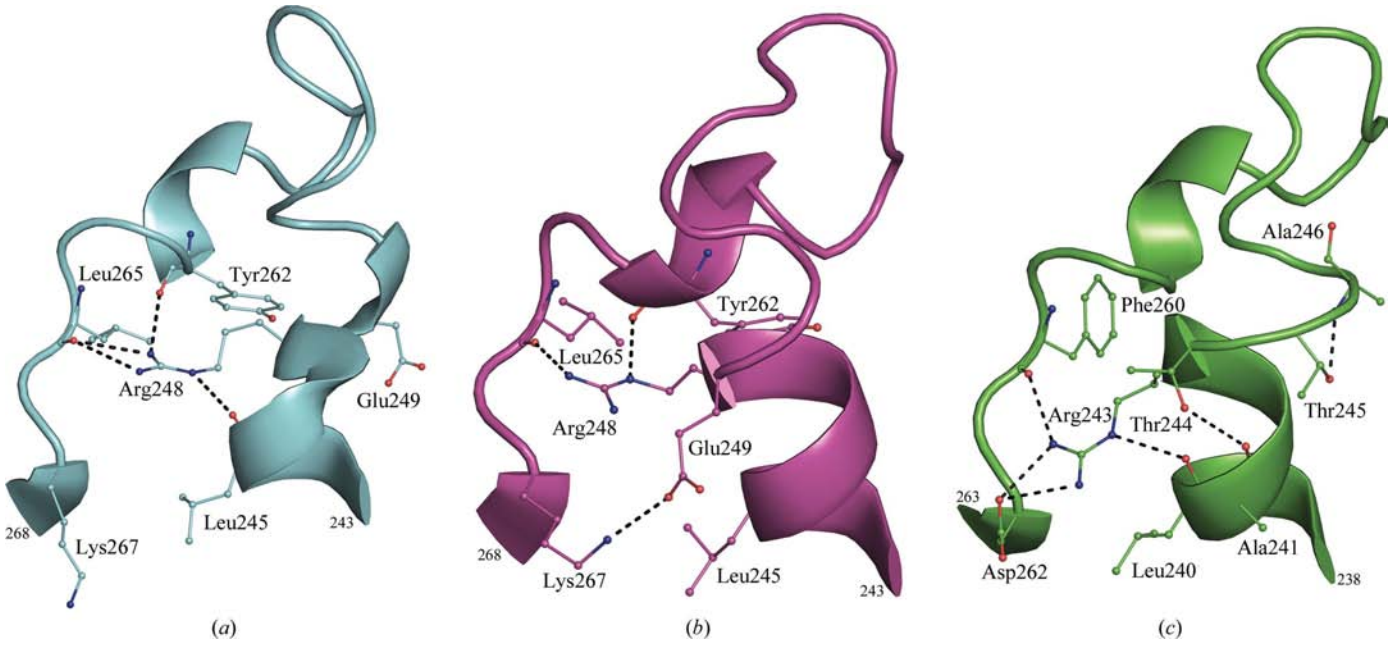

Figure 9
Conformation of the pantothenate-binding region in the structures of *Ec*PanK and *Mt*PanK. (*a*) *Ec*PanK in the absence of bound pantothenate. (*b*) *Ec*PanK with bound pantothenate. (*c*) The intermediate complex of *Mt*PanK.

indicative. The distribution of charges around the reacting groups is also in consonance with the indication provided by the distance criteria. In *Ec*PanK, the density of positive charges around the γ-phosphate of the bound ATP analogue is much greater in comparison to that in *Mt*PanK. The large number of positive charges around the γ-phosphate of ATP would aid in neutralizing the excess negative charge that would develop on the O atoms upon the formation of a trigonal bipyramidal phosphorane transition state. These structural features indicate that although the mechanism is predominantly associative in both the enzymes, the dissociative component is perhaps higher in *Mt*PanK than in *Ec*PanK.

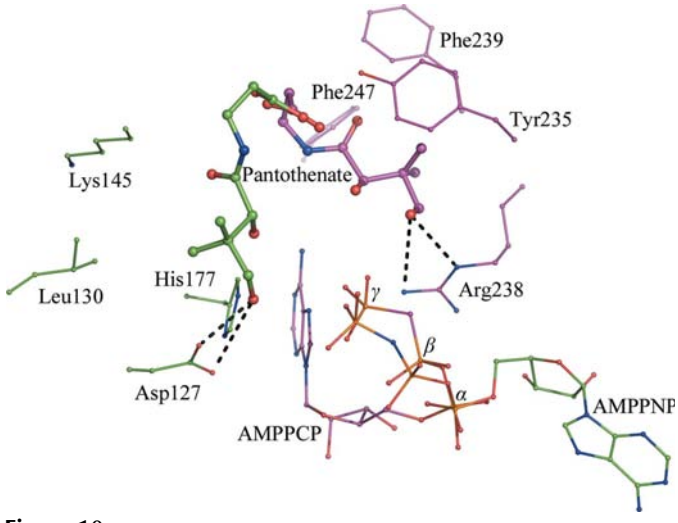

Figure 10
Binding site of pantothenate and its relative spatial location in *Mt*PanK and *Ec*PanK. The bound pantothenate, ATP analogue and pantothenate-binding residues in *Mt*PanK and *Ec*PanK are depicted in magenta and green colours, respectively. The figure was obtained by superposition of the relevant *Mt*PanK and *Ec*PanK structures.

The changes in location of the ligands apparently associated with the action of *Mt*PanK is remarkable and to the best of our knowledge such changes have not been observed so far in other enzymes. They are also interesting because two highly homologous enzymes, *Ec*PanK and *Mt*PanK, exhibit such remarkable differences in the location of ligands and local conformation during action. It is gratifying that these differences can be understood substantially in terms of local conformational changes caused by a few key substitutions. However, the results should be treated with caution as they are unexpected and counterintuitive. The possibility that the changes in ligand positions were caused by crystal packing was carefully examined. While some of the residues in the ligand-binding regions are involved in intermolecular contacts, the observed conformation of *Mt*PanK and the conformation with the modifications found in *Ec*PanK are compatible with the crystal structure. (In contrast, *Ec*PanK molecules with two different conformations for the binding regions are compatible only with their respective crystal structures.) Furthermore, as mentioned earlier, *Mt*PanK complexes prepared by soaking and cocrystallization gave identical results. Thus, the observed differences do not appear to have been caused by crystal packing, although such a possibility can never be entirely ruled out.

The difference in the location of nucleotides in the initiation and end complexes raises questions regarding the nature of ATP-binding sites in proteins. In an early study based on the then available crystal structure, the protein recognition of adenylate was described as 'fuzzy' (Moodie *et al.*, 1996). Subsequent studies have confirmed this fuzziness (Denessiouk *et al.*, 2001; Pyrkov *et al.*, 2007). Most of the specific hydrophilic

interactions involve the phosphates and some involve ribose. Adenine has a largely hydrophobic interface and hydrogen bonds involving adenine are scarce. There is no conserved hydrogen-bonding pattern for adenine recognition. Stacking of an aromatic residue, in addition to the hydrophobic contacts, is a characteristic feature of adenine recognition. As is clear from the results presented earlier, adenines binding in *Mt*PanK and *Ec*PanK complexes are compatible with these characteristics. A comparative study of the binding sites of adenine and guanine in the relevant protein complexes has also been carried out (Nobeli *et al.*, 2001). There are differences in the clustering of amino-acid residues around the two bases. However, the clustering around guanine is also described as fuzzy. Thus, fuzziness is a description that occurs when dealing with the binding of adenine as well as guanine. Interestingly, *Ec*PanK is active at a 19% level when GTP is used instead of ATP (Vallari *et al.*, 1987). Thus, the specificity for the nucleotide base in the enzymes concerned, including PanK, is not very stringent. Changes in the location of the base in the binding site are consistent with this observation. Thus, while the influence of artifacts on the results presented here cannot be ruled out, the implications of the remarkable difference in the action of *Mt*PanK and *Ec*PanK suggested by these results, including those for inhibitor design aimed at drug development, merit serious consideration and further exploration.

The data sets used in the present work were collected at the X-ray facility for Structural Biology at the Institute, supported by the Department of Science and Technology (DST). Computations were performed at the Super Computer Education and Research Centre of the Institute and the Bioinformatics Centre and Graphics Facility, both supported by the Department of Biotechnology (DBT). This work was supported by a Distinguished Biotechnologist Award to MV from the DBT and a DBT research grant to AS. BC is a CSIR research fellow.

References

Brand, L. A. & Strauss, E. (2005). *J. Biol. Chem.* **280**, 20185–20188.

Brünger, A. T., Adams, P. D., Clore, G. M., DeLano, W. L., Gros, P., Grosse-Kunstleve, R. W., Jiang, J.-S., Kuszewski, J., Nilges, M., Pannu, N. S., Read, R. J., Rice, L. M., Simonson, T. & Warren, G. L. (1998). *Acta Cryst.* D**54**, 905–921.

Cheek, S., Ginalski, K., Zhang, H. & Grishin, N. V. (2005). *BMC Struct. Biol.* **5**, 6–24.

Choudhry, A. E., Mandichak, T. L., Broskey, J. P., Egolf, R. W., Kinsland, C., Begley, T. P., Seefeld, M. A., Ku, T. W., Brown, J. R., Zalacain, M. & Ratnam, K. (2003). *Antimicrob. Agents Chemother.* **47**, 2051–2055.

Cohen, G. E. (1997). *J. Appl. Cryst.* **30**, 1160–1161.

Collaborative Computational Project, Number 4 (1994). *Acta Cryst.* D**50**, 760–763.

Das, S., Kumar, P., Bhor, V., Surolia, A. & Vijayan, M. (2005). *Acta Cryst.* F**61**, 65–67.

Das, S., Kumar, P., Bhor, V., Surolia, A. & Vijayan, M. (2006). *Acta Cryst.* D**62**, 628–638.

Davis, I. W., Leaver-Fay, A., Chen, V. B., Block, J. N., Kapral, G. J., Wang, X., Murray, L. W., Arendall, W. B. III, Snoeyink, J., Richardson, J. S. & Richardson, D. C. (2007). *Nucleic Acids Res.* **35**, W375–W383.

DeLano, W. L. (2002). *The PyMOL Molecular Graphics System.* De Lano Scientific, San Carlos, California, USA.

Denessiouk, K. A., Rantanen, V. V. & Johnson, M. S. (2001). *Proteins*, **44**, 282–291.

Dundas, J., Ouyang, Z., Tseng, J., Binkowski, A., Turpaz, Y. & Liang, J. (2006). *Nucleic Acids Res.* **34**, W116–W118.

Emsley, P. & Cowtan, K. (2004). *Acta Cryst.* D**60**, 2126–2132.

Geerlof, A., Lewendon, A. & Shaw, W. V. (1999). *J. Biol. Chem.* **274**, 27105–27111.

Hong, B. S., Senisterra, G., Rabeh, W. M., Vedadi, M., Leonardi, R., Zhang, Y. M., Rock, C. O., Jackowski, S. & Park, H. W. (2007). *J. Biol. Chem.* **282**, 27984–27993.

Ivey, R. A., Zhang, Y. M., Virga, K. G., Henever, K., Lee, R. E., Rock, C. O., Jackowski, S. & Park, H. W. (2004). *J. Biol. Chem.* **279**, 35622–35629.

Kabsch, W. & Sander, C. (1983). *Biopolymers*, **22**, 2577–2637.

Kennard, O., Isaacs, N. W., Motherwell, W. D. S., Copolla, J. C., Wampler, D. L., Larson, A. C. & Watson, D. G. (1971). *Proc. R. Soc. London Ser. A*, **325**, 401–436.

Krishna, R., Prabu, J. R., Manjunath, G. P., Datta, S., Chandra, N. R., Muniyappa, K. & Vijayan, M. (2007). *J. Mol. Biol.* **367**, 1130–1144.

Ku, S. Y., Cornell, K. A. & Howell, P. L. (2007). *BMC Struct. Biol.* **7**, 70.

Laskowski, R. A., Moss, D. S. & Thornton, J. M. (1993). *J. Mol. Biol.* **231**, 1049–1067.

Leonardi, R., Zhang, Y. M., Rock, C. O. & Jackowski, S. (2005). *Prog. Lipid Res.* **44**, 125–153.

Mildvan, A. (1997). *Proteins*, **29**, 401–416.

Moodie, S. L., Mitchell, J. B. O. & Thornton, J. M. (1996). *J. Mol. Biol.* **263**, 486–500.

Navaza, J. (1994). *Acta Cryst.* A**50**, 157–163.

Nobeli, I., Laskowski, R. A., Valdar, W. S. J. & Thornton, J. M. (2001). *Nucleic Acids Res.* **29**, 4294–4309.

Otwinowski, Z. & Minor, W. (1997). *Methods Enzymol.* **276**, 307–326.

Pyrkov, T. V., Kosinsky, Y. A., Arseniev, A. S., Priestle, J. P., Jacoby, E. & Efremov, R. G. (2007). *Proteins*, **66**, 388–398.

Roy, S., Saraswathi, R., Chatterji, D. & Vijayan, M. (2008). *J. Mol. Biol.* **375**, 948–959.

Schüttelkopf, A. W. & van Aalten, D. M. F. (2004). *Acta Cryst.* D**60**, 1355–1363.

Selvaraj, M., Roy, S., Singh, N. S., Sangeetha, R., Varshney, U. & Vijayan, M. (2007). *J. Mol. Biol.* **372**, 186–193.

Song, W. J. & Jackowski, S. (1994). *J. Biol. Chem.* **269**, 27051–27058.

Vallari, D. S., Jackowski, S. & Rock, C. O. (1987). *J. Biol. Chem.* **262**, 2468–2471.

Vijayan, M. (2005). *Tuberculosis*, **85**, 357–366.

Yang, K., Eyobo, Y., Brand, L. A., Martynowski, D., Tomchick, D., Strauss, E. & Zhang, H. (2006). *J. Bacteriol.* **188**, 5532–5540.

Yun, M., Park, C. G., Kim, J. Y., Rock, C. O., Jackowski, S. & Park, H. W. (2000). *J. Biol. Chem.* **275**, 28093–28099.

Zhang, Y. M., Rock, C. O. & Jackowski, S. (2006). *J. Biol. Chem.* **281**, 107–114.

Zhou, B., Westaway, S. K., Levinson, B., Johnson, M. A., Gitschier, J. & Hayflick, S. J. (2001). *Nature Genet.* **28**, 345–349.